ROYAL SOCIETY
OF CHEMISTRY

PAPER

Check for updates

Reliable *I/V* characteristics and long lifetime of porphyrin-based single-molecule junctions†

Xinlei Yao,[a] Maxime Vonesch, [b] Lihao Guan,[a] Jennifer Wytko, [b] Jean Weiss, [b] Xiaonan Sun [a] *[a] and Jean-Christophe Lacroix [a] *[a]

In this work diamino-porphyrin derivatives, in their free base or cobalt complex forms, have been used to construct SMJs. Porphyrin oligomers were covalently bonded to a bottom electrode by diazonium cation electroreduction and a STM tip was used to complete the junction. Conductance *versus* time (*G*(*t*)) measurements reveal stable SMJs with lifetimes as long as 70 s, attributable to the diazonium bonding procedure and the amino anchoring groups. SMJ conductance was studied statistically by three methods: the STM-bj $G_{histo}(d)$ histograms, STM $G_{time}(t)$ and voltage-dependent $G_{volt}(V)$ heat maps. Conductance and attenuation factors (β) for Co or free-base porphyrin SMJs, compared by the three methods, are fully consistent, length-dependent and show a strong molecular signature. Trends in the variation of the attenuation factors *versus* voltage indicate a voltage-driven β decrease for both types of SMJ.

Introduction

With electronic devices continuously shrinking,[1,2] resolution approaching a few nanometers[3] and the introduction of vertically aligned field-effect transistors,[4,5] two-terminal vertical single-atom or single-molecule devices may soon become a realistic alternative to silicon-based devices. Two-terminal atomic switches,[6] in which a single atom connects and disconnects two electrodes have already been proposed as an emerging memory technology.[7,8] Such redox-active devices can be reversibly switched at potentials below 1 V[9] and are thus capable of saving a great deal of the energy used in data storage compared to present technologies.[10] Two terminal molecular junctions (MJs), in which molecules are connected between two electrodes, are also proposed as potential building-blocks in nanoelectronics.[11–19] Large-area MJs and single molecule junctions (SMJs) have allowed investigation of electron transport properties at complementary scales,[20–25] and specific MJs show functional conductance switching behaviours triggered by bias,[26] redox reactions,[27] or light.[28,29] Current *versus* potential curves characterize MJ transport properties and depend mainly on the molecules used, on the distance between the electrodes and on the coupling of the molecules to the contacts.[30–33]

The most popular method for generating SMJs is the scanning tunneling microscopy-break junction (STM-bj) technique.[34] Most STM-bj studies report the molecular conductance at a fixed and small bias, and *I/V* curves are not systematically reported,[35–44] as STM-based SMJs have proved to be unstable. The mechanically controlled break junction (MC-bj) is an alternative method where horizontal SMJs are generated in a nanogap between two electrodes.[45–47] SMJs generated by MC-bj are more stable,[48–51] and *I/V* measurements on such devices have been reported.[52,53] SMJs built using all carbon electrodes have been a new tendency[54–57] where the constructed SMJs, allowed the development for studying various effects on transport[58,59] and for monitoring physical and chemical processes at the single-molecule level.[60,61]

Current *versus* time curves during SMJ formation have also been measured using STM-bj and MC-bj set-ups and nano-gapped graphene point-contact arrays. When a STM set-up is used, the tip is first brought up to a conductive surface using a tunneling set-point to fix the distance between the tip and the surface. Then the feedback is switched off and the current *versus* time curve is recorded. If a molecule bridges the gap between the tip and the surface, an SMJ is obtained, and its formation can be observed as a typical telegraph signal between two states corresponding to ON (SMJ created) and OFF (no SMJ) current.[62–65] This is often referred to as an STM "blinking" experiment where a short lifetime of less than a second is generally recorded at room T. In most publications the molecule is in solution and remains mobile, as it is still in contact with a liquid environment. This and the natural drift of the tip

---

[a] Université de Paris Cité, ITODYS, CNRS-UMR 7086, 15 rue Jean-Antoine de Baïf, 75205 Paris Cedex 13, France. E-mail: sun.xiaonan@u-paris.fr, lacroix@u-paris.fr

[b] Institut de Chimie de Strasbourg, CNRS-UMR 7177, Université de Strasbourg, 4, rue Blaise Pascal, 67000 Strasbourg, France

† Electronic supplementary information (ESI) available: Free of charge. It includes details of STM-bj current traces and conductance histograms, CV curves and thickness characterization by AFM scratching. See DOI: https://doi.org/10.1039/d3tc04142e

4326 | *J. Mater. Chem. C*, 2024, **12**, 4326–4335

This journal is © The Royal Society of Chemistry 2024

provoke instability and the breaking of the junction. A successful improvement of this technique was recently reported using electrochemistry to form both ends of the SMJs with Au–C and Si–C molecule–electrode contacts; this extends the SMJ lifetime to as long as around 1 second.[66,67] Recently, we reported SMJs generated using a strategy, where molecules are first immobilized in a compact layer on a surface by means of diazonium electroreduction.[68] In this way, the individual molecular mobility was suppressed. STM-based SMJs were easily generated and the tip was stabilized in contact with a single immobilized grafted oligomer for as long as 10 seconds for SMJs generated from 5-aminophenyl-15,20-diphenylporphyrin (TPP-NH$_2$) and its corresponding Co(II) complex, (CoTPP-NH$_2$).[69]

The present work reports the fabrication and the characterization, using a STM set-up, of porphyrin-based SMJs from 5,10-diaminophenyl-15,20-diphenylporphyrin (H$_2$N-TPP-NH$_2$) and its corresponding Co(II) complex, (H$_2$N-CoTPP-NH$_2$). One of the amino groups serves as precursor for diazonium electroreduction on the bottom electrode as in our previous study[69] and the other acts as additional anchor for the Au STM-tip top-electrode (Fig. 1). Porphyrin oligomers were thus covalently bonded to the bottom electrodes by diazonium electroreduction[70–72] and a STM tip was used to complete the junctions. The stability and charge transport properties of the SMJs derived from these molecules are compared with those obtained from TPP-NH$_2$ and CoTPP-NH$_2$ SMJs[69] and underline the effect of the additional top NH$_2$ terminal. We show that the SMJs lifetime is improved and can reach a minute, which makes I/V characterization easy to perform at the single-molecule level. SMJ conductance was statistically studied by three methods: the STM-bj $G_{histo}(d)$ histogram, STM $G_{time}(t)$ and voltage-dependent $G_{volt}(V)$ measurement. Attenuation factors (β) were investigated and compared for Co and free-base porphyrin SMJs using the three methods. Thanks to the I/V characteristics, attenuation trends versus voltage were plotted at

the single-molecule level and a voltage-driven β decrease was evidenced and analyzed.

Results and discussion

Immobilization and characterization of the grafted oligomers

The free base, 5,10-diaminophenyl-15,20-diphenylporphyrin H$_2$N-TPP-NH$_2$,[73] and its corresponding Co(II) complex, H$_2$N-CoTPP-NH$_2$,[74] were synthesized by known procedures. The two molecules have identical structures (AMPAC-calculated molecular length of 2.2 nm) except for the presence or absence of the coordinated transition metal ion. Detailed electrochemical properties of H$_2$N-TPP-NH$_2$ and H$_2$N-CoTPP-NH$_2$ in solution are described in the ESI† (Fig. S1–S3). [TPP]$_n$ or [CoTPP]$_n$ (n = 1–3) oligo-porphyrins of controlled thickness were grafted onto ultra-flat gold substrates (deposited on Si/SiO$_2$ wafers) by diazonium cation electroreduction. The diazonium derivatives were first generated in situ by adding 15 equivalents of t-butyl-nitrite (tBuNO2)[75–77] then reduced by sweeping the potential ranges applied on the gold electrode (the number of scans is varied: Table S1, ESI†). The [CoTPP]$_n$-modified electrode was then studied by cyclic voltammetry (CV) limited to the reduction process centred on the Co ion. The CV curve (Fig. S1, ESI†) shows the reversible reduction wave at $E_{1/2}$= −0.9 V ($\Delta E_p \approx$ 0 V at low scan rates). The shape of this signal is characteristic of immobilized electroactive species and indicates that the film deposited is very stable. Integration of the redox peaks yields an apparent surface concentration (Fig. S1 and Table S1, ESI†), showing that the grafted films are based on oligomers (variable n-mers) of [CoTPP]. By the AFM scratch technique[78] (Fig. S2 and S3, ESI†), average thicknesses of 2.5 ± 1 nm (n = 1–2), 4.5 ± 1 nm (n = 2–3), and 6.5 ± 1 nm (n = 3–4) were found for [TPP]$_n$ or [CoTPP]$_n$.

XPS was also used to characterize the 2.5 ± 1 nm monolayers (Fig. S4, ESI†). Briefly, the C$_{1s}$, N$_{1s}$ and Co$_{2p}$ signals indicate that the porphyrin structure is unaffected by the electrochemical grafting. The cobalt signal consists of two peaks at 780.4 eV and 796 eV that correspond to Co$_{2p3/2}$ and Co$_{2p1/2}$. The splitting and the positions of the peaks indicate that the cobalt is in the +2 oxidation state.[79] The N$_{1s}$ signal is observed with two peaks at 399 eV and 400.5 eV. The first one is due to a porphyrin unit bound to a metal center[80] (here cobalt) whereas that at 400.5 eV can be attributed to free amino groups.[81] The ratio of nitrogen at 399 eV to cobalt is 3.5, close to the theoretical value of 4 (and indicating that most of the porphyrin units are complexed to a cobalt center) whereas the ratio of nitrogen at 399 eV to nitrogen at 400.5 eV is 4 and suggests that this monolayer is terminated by an amino group (Fig. 1b). To check this point, monolayers generated using mono-amino-porphyrins (5-(p-aminophenyl)-10,15,20-triphenylporphyrins) were deposited on gold and analyzed by XPS. The N$_{1s}$/Co$_{2p}$ atomic ratio is again 3.5 but the nitrogen signal shows only one peak at 399 eV and no peak at 400.5 eV. The overall ratio of N$_{1s}$/Co$_{2p}$ is thus 3.5 and 4.5 when the monolayers are generated from cobalt mono-amino-porphyrin and diamino-porphyrin precursors, respectively, which
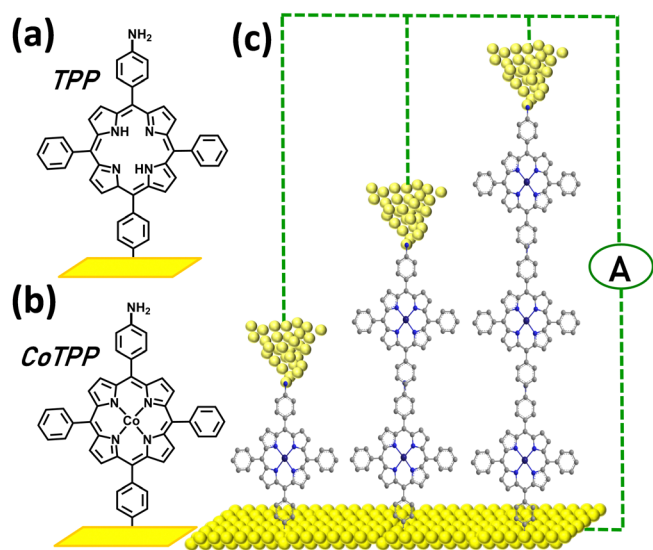

Fig. 1 Diazonium-based porphyrin SMJs: (a) and (b) Scheme of MTPP building blocks grafted on the bottom electrode where M is cobalt(II) or 2H (c) Scheme of Au-[CoTPP]$_n$-Au SMJs, n = 1–3.

This journal is © The Royal Society of Chemistry 2024

J. Mater. Chem. C, 2024, 12, 4326–4335 | 4327

confirms that, in marked contrast with the oligomers studied in ref. 68, 69, an extra amino group terminates the layers generated from cobalt diamino-porphyrin building blocks.

The compact layers of grafted oligomers of different lengths, covalently C–Au bonded perpendicularly to the bottom electrode, were used to construct stable SMJs using an STM set-up, and several methods were used to investigate transport properties.

STM-bj conductance measurements of grafted cobalt(II) p-aminophenylporphyrin

The first method is the widely used STM-bj technique.[34] The STM tip is repeatedly driven into or pulled out of contact with the preformed oligomers, and the current through an Au-molecule-Au SMJ is recorded at a low bias voltage (<0.2 V). The current plateau in the conductance versus distance ($G(d)$) traces during this process indicate the formation of an SMJ. Hundreds of $G(d)$ traces with plateaus are selected to construct a histogram giving a most probable average conductance value for the many unstable SMJs obtained. The conductance values measured by the STM-bj technique are defined as G_{histo}. Typical $G(d)$ traces with plateaus (Fig. 2a and Fig. S5 and S6, ESI†) whose lengths range from 3 Å to 1 nm clearly indicate that Au-[CoTPP]$_n$-Au SMJs are formed (length-conductance two-dimensional histograms of the generated SMJs are shown in

Fig. S7, ESI†). Fig. 2b shows the Au-[CoTPP]$_1$-Au SMJ conductance histogram constructed from hundreds $G(d)$ traces at a low bias voltage (0.025 V). High-(HC) and low-conductance (LC) peaks are visible in the histogram with values centred at 2.5 and 5.3×10^{-3} G_0, respectively, where G_0 is the quantum conductance. The CoTPP oligomers do not support conformational switches or changes of junction geometry due to stretching.[30,82,83] The HC and LC peaks observed, with a small conductance shift of less than half an order of magnitude, can most likely be attributed to different molecule/electrode (π- or σ-) contact geometries as already observed by many groups.[84–87] The LC peak is always stronger and gives the main conductance value, whereas the HC peak is often broader and weaker.

STM-$G(t)$ experiments on grafted cobalt(II) p-aminophenylporphyrin

In this second method, different from the bj technique, the conductance versus time ($G(t)$) traces are recorded at a fixed tip-surface distance (STM feedback off). These $G(t)$ traces characterize not only the average conductance (defined as G_{time}) of the SMJ but also the limited lifetime during which a molecule bridges the gap between the two electrodes. The telegraph $G(t)$ signals observed in Fig. 2c and Fig. S8 (ESI†) demonstrate the alternating formation (state ON) and breakdown (state OFF) of an Au-[CoTPP]$_1$-Au SMJ (Fig. 2d). Each "ON" conductance

Fig. 2 (a) Conductance $G(d)$ traces of Au–[CoTPP]$_1$-Au SMJs (b) $G(d)$ histogram for Au–[CoTPP]$_1$-Au SMJ. Set point: $I_t = 1$ nA; $U_s = 0.025$ V. (c) $G(t)$ traces from Au–[CoTPP]$_1$-Au junction. Set-point: $I_t = 1$ nA; $U_s = 0.05$ V: (d) Scheme showing the SMJ ON (tip in contact with the molecule) or OFF (tip not in contact) states inducing conductance vs. time telegraph signals. (e) $G(t)$ trace showing stabilization of a SMJ with lifetime of 70 s; $G(t)$ blinks between the LC and HC states without junction breakdown.

4328 | J. Mater. Chem. C, 2024, **12**, 4326–4335

This journal is © The Royal Society of Chemistry 2024

plateau lasts initially a very short time (less than 0.5 s in Fig. S8, ESI†). This phenomenon is often referred to as SMJ "blinking".[61,67] The conductance in the ON state is 2.5×10^{-3} G_0 (Fig. 2c) and corresponds to the LC state of the STM-bj histograms. Moreover, the SMJ "blinks" for about 15 s in this experiment. Such a long cycle of repeating ON/OFF alternations has very rarely been observed for STM-generated SMJs and could indicate a tendency to form more stable SMJs. Fig. 2e shows another experiment in which the junction stabilizes after a short initial blinking period. In this typical $G(t)$ trace (Fig. 2e) the conductance is initially close to zero (STM tunneling setpoint) as the SMJ is not yet formed but then jumps and stabilizes around two distinct values of 2.5×10^{-3} G_0 or 5.6×10^{-3} G_0. The long conductance plateaus in Fig. 2e (with two distinct values) indicates the formation of an individual Au-[CoTPP]$_1$-Au SMJ. The two different conductance plateaus can be identified as the HC and LC states, which are consistent with those identified by G_{histo} from STM-bj experiments (Fig. 2a). An important result is the observation for the very first time of an Au-[CoTPP]$_1$-Au SMJ generated with a STM setup, with a lifetime as long as 70 s before total breakdown. More $G(t)$ traces with lifetimes of tens of seconds were easily obtained (Fig. S9, ESI†), which indicates that the long lifetime of the SMJs is reproducible. Alternations between the LC and HC states during the long duration of the SMJ (Fig. 2e and Fig. S9, ESI†) are attributed to the variation of tip-molecule contact geometry.[84–86] Interestingly, the SMJ does not break down, despite the LC and HC fluctuation. The SMJ LC plateau lasts around 55 s in total, much longer than that for HC (15 s) which indicates that the LC state is preferred. Moreover, the LC and HC fluctuation shows that SMJs fabricated using layers

generated by diazonium electroreduction are a good platform for monitoring molecular physical and chemical processes at the single-molecule level very similar to nanogapped graphene point-contact arrays.[55,61]

G_{histo} and G_{time} heat maps of free base and cobalt(II) p-aminophenylporphyrin oligomers

The Au-[CoTPP]$_n$-Au and the Au-[TPP]$_n$-Au SMJs have exactly the same configurations and terminal groups except for the presence or absence of the coordinated metal ion. Comparison of the two SMJs clearly reflects the influence of the cobalt center on the SMJ transport behavior. By means of the STM-bj technique, typical $G(d)$ traces with visible plateaus are displayed (Fig. S5 and S6, ESI†), indicating SMJ formation. Conductance histograms, constructed from hundreds of such $G(d)$ traces, indicate the most probable conductance values. Fig. 3a and e shows the combined conductance histograms from both Au-[CoTPP]$_n$-Au and Au-[TPP]$_n$-Au SMJs, respectively, for three different length (n = 1, 2, 3). Values of G_{Histo} for the Au-[CoTPP]$_n$-Au SMJs are around 2.6×10^{-3} G_0, 1.8×10^{-3} G_0 and 1.1×10^{-3} G_0 for n = 1, 2, and 3, respectively (Fig. 4a inset). Corresponding values for the Au-[TPP]$_n$-Au SMJs are 3.2×10^{-3} G_0 (n = 1), 1.1×10^{-3} G_0 (n = 2) and 2×10^{-4} G_0 (n = 3) (Fig. 3e inset). Note that HC and LC states are not easily detected in the G_{Histo} measured with the [TPP]$_n$ oligomers.

$G(t)$ measurements have been performed for all these systems and are reported in Fig. S10 and S11 (ESI†) (the lifetimes of these SMJs are all around 1 min). With our strategy of SMJ fabrication, individual SMJs can be stabilized easily with lifetimes of tens of seconds. Two-dimensional (2D) $G(t)$ heat maps for many SMJs, each constructed from hundreds of traces, have
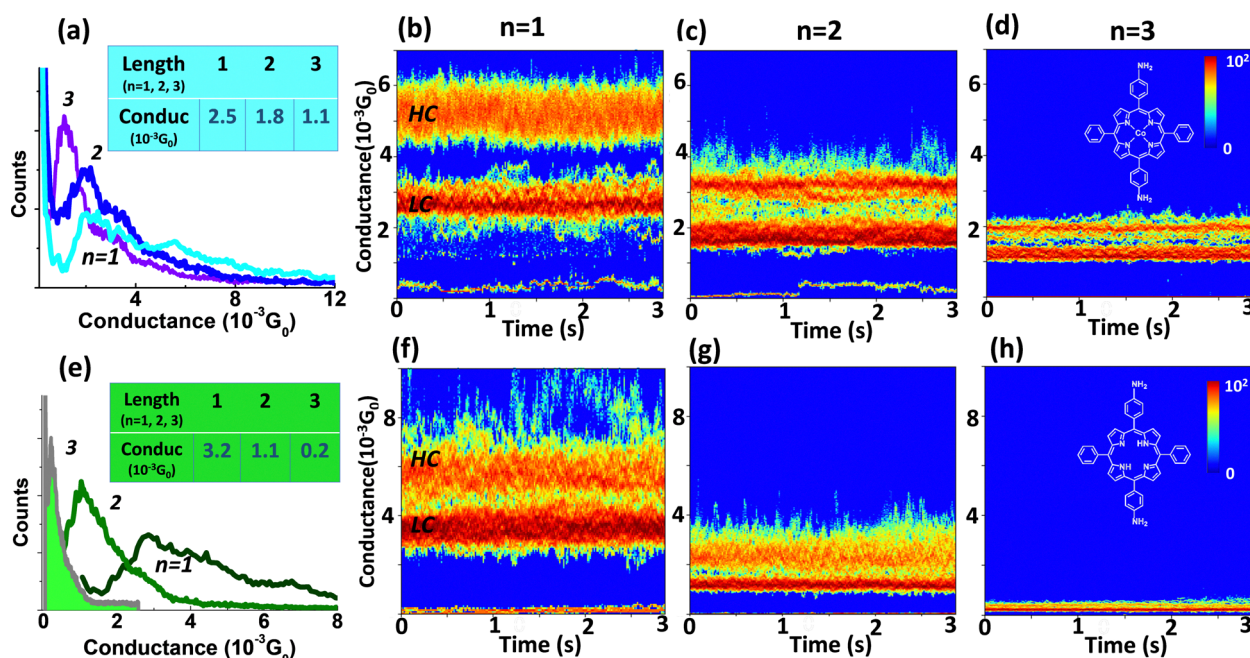

Fig. 3 Combined STM-bj histograms: (a) Au-[CoTPP]$_n$-Au and (e) Au-[TPP]$_n$-Au SMJs (n = 1–3). Inset tables indicate the conductance values. (b)–(d), (f)–(h) G_{time} 2D heat maps for both SMJs with different junction lengths (n = 1–3).

This journal is © The Royal Society of Chemistry 2024
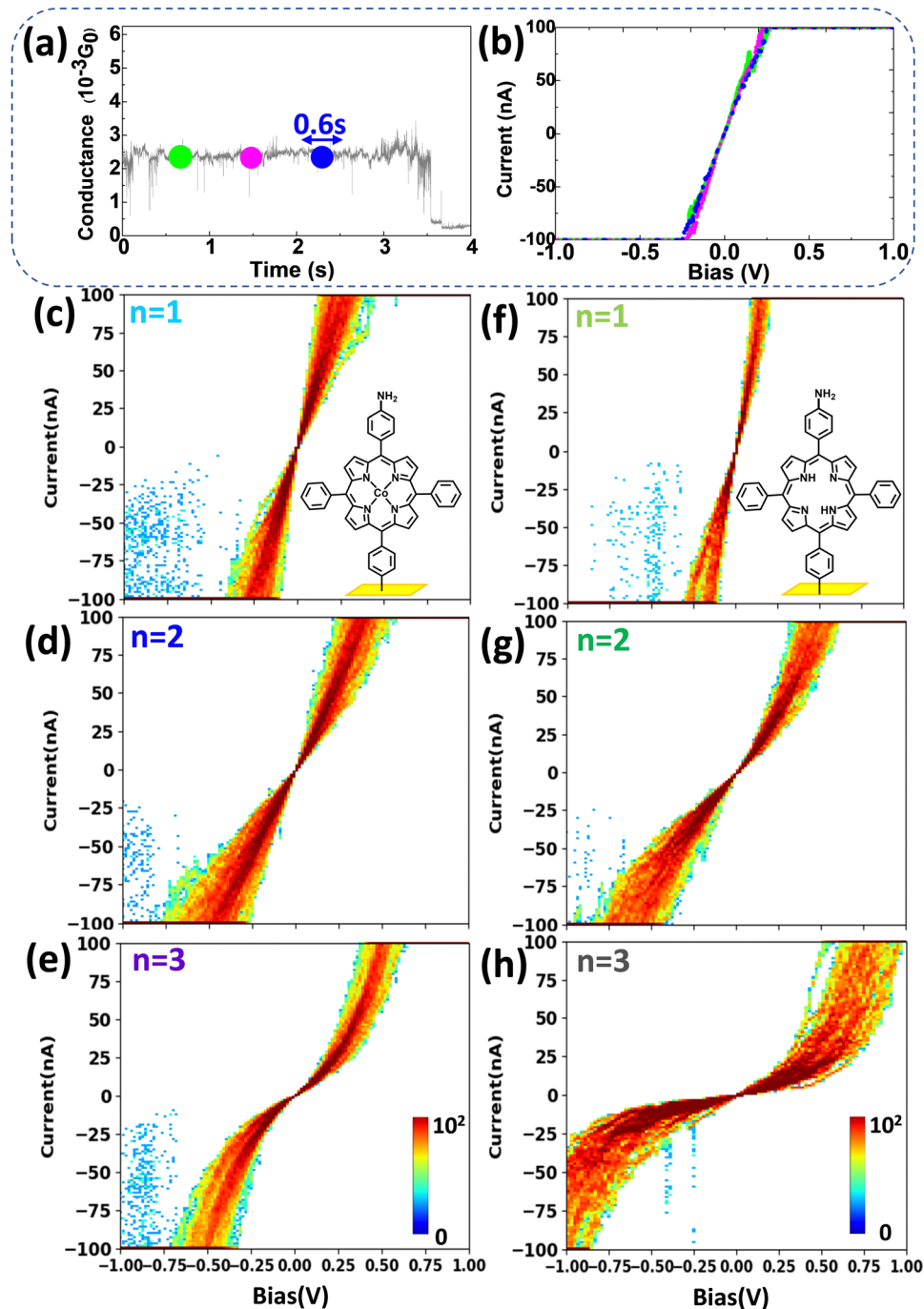
J. Mater. Chem. C, 2024, **12**, 4326–4335 | **4329**

Fig. 4 In-depth I/V characteristics of SMJs: (a) typical Au-[CoTPP]$_1$-Au G(t) trace; the colored dots indicate the 0.6 s time for an I/V measurement. (b) Three different I/V traces from junctions of (a). 2D I/V heat maps for (c)–(e) Au-[CoTPP]$_n$-Au and (f)–(h) Au-[TPP]$_n$-Au junctions of different lengths, n = 1, 2, 3, respectively.

been obtained and are displayed with a 3 s time window (Fig. 3). In Fig. 3b–d, the Au-[CoTPP]$_n$-Au G(t) heat maps for SMJs of different lengths show clearly two distinct conductance values, distinguished again as the LC and HC states. The conductance values from the initial STM tunneling set-points are visible as a bottom heat line. The LC states are always 'hotter' than the HC states for the three SMJs (Fig. 3b–d). These results are in agreement with the STM-bj observations, where the LC peaks

are stronger than the HC peaks (when observed) and are the main conductive states. These observations also confirm that LC and HC states are obtained with all SMJs, which is not always obvious from the STM-bj histograms of Fig. 3a and e. Both the G_{histo} and the G_{time} heat map analyses indicate that Au-[CoTPP]$_n$-Au SMJs transport charge efficiently, with rather high conductance values (10^{-3} G_0) which fall relatively slowly as the junction length increases.

4330 | J. Mater. Chem. C, 2024, 12, 4326–4335

This journal is © The Royal Society of Chemistry 2024

The 2D G_{time} heat maps from the Au-[TPP]$_n$-Au SMJs are displayed in Fig. 3f and h; the LC and the HC states are again distinguishable, and the conductance values in good agreement with the G_{histo} results. However, the conductance of the Au-[TPP]$_1$-Au SMJ is surprisingly higher ($3.5 \times 10^{-3} G_0$) than that of the Au-[CoTPP]$_1$-Au SMJ ($2.6 \times 10^{-3} G_0$).[48,64,88–90] In the case of longer SMJs, the conductance values (both G_{time} and G_{histo}) of Au-[CoTPP]$_n$-Au are greater than those of the Au-[TPP]$_n$-Au ($n = 2, 3$). The Au-[TPP]$_n$-Au SMJs show a faster conductance fall-off with the oligomer length, and both G_{histo} and G_{time} decrease by more than one order of magnitude (from 10^{-3} to $10^{-4} G_0$). This indicates that the coordinated Co metal center has a strong impact on the conductance and promotes charge transport more efficiently over a greater distance (6 nm) than the free base. We attribute this phenomenon to the HOMO and LUMO of [CoTPP]$_n$ being closer to the gold Fermi level than those of the [TPP]$_n$, which is in line with the electrochemical results (Fig. S12, ESI†). The SMJ 2D $G(t)$ heat map has been very rarely achieved; it provides statistical information about SMJ conductivity and stability. Our result reveals that G_{time} measurement and the corresponding heat maps can be used as an effective and reliable method for SMJ characterization.

I/V measurements

To go a step further, it is important to study the voltage-dependence of charge transport, *i.e.* to perform I/V measurements at the single-molecule level, which is usually difficult, despite its intrinsic role in the understanding of molecular electronics.

The results in Fig. 2 and 3 demonstrate that we can easily stabilize a molecule between the STM tip and the bottom electrode for a long time (tens of seconds). Once stabilized on the $G(t)$ plateau, the applied bias voltage can be swept, and the current measured so that SMJ I/V curves are obtained. For example, for an Au-[CoTPP]$_1$-Au SMJ, during the 4 s $G(t)$ plateau (Fig. 4a), I/V curves (each lasting about 0.6 s) can be easily measured in the −1 to +1 V voltage range (Fig. 4b). By repeating

the procedure, we record hundreds of I/V curves and construct 2D I/V heat maps on both Au-[CoTPP]$_n$-Au and Au-[TPP]$_n$-Au SMJs of different junction lengths (Fig. 4c–e and f–h, and Fig. S13, ESI† for an overlay). The I/V characteristics are easily accessible and are clearly reproducible in our case thanks to the high SMJ stability, although single-molecule level I/V measurements are known to be challenging. For both types of SMJs, the I/V curves rise linearly with the bias voltage within a small voltage range (<0.2 V) and then increase more rapidly (non-linear increase) at higher voltages. Another important observation is that the 2D I/V characteristics of Au-[CoTPP]$_n$-Au SMJs depend less on the junction length than those of Au-[TPP]$_n$-Au SMJs. This demonstrates again the strong influence of the Co cation on SMJ conductance.

Attenuation plots by the three methods

The attenuation plot (or β plot) is defined by $G = G_0 e^{-\beta d}$ where G_0 is the pre-exponential factor and d is the junction length. It characterizes the conductance dependence on the molecular junction length and reveals key differences in transport mechanisms.[22,32,91–95] The β values (at low bias) for the Au-[CoTPP]$_n$-Au and Au-[TPP]$_n$-Au SMJs, calculated from the different $G(d)$ (STM-bj histograms), $G(t)$ (stabilized SMJ conductance) and $G(V)$ (calculated from the current (of the I/V curve) divided by the corresponding voltage) methods in Fig. 5a–c are defined in what follows as β_d, β_t and β_V, respectively.

First, using the STM-bj method, a β_d value around 0.25 ± 0.1 nm^{-1} is obtained for Au-[CoTPP]$_n$-Au SMJs (LC states) (red plot in Fig. 5a), while a value around 0.68 ± 0.1 nm^{-1} is found for Au-[TPP]$_n$-Au SMJs (blue plot in Fig. 5a). (The HC states being not clearly observed for all n-mers by the STM-bj methods are not displayed in Fig. 5a). The applied bias voltages for measuring the conductance are very small (0.025 to 0.1 V) and are thus within the linear I/V range, as discussed above. Second, β_t values are calculated from the stable $G(t)$ traces in Fig. 3 and β_t values for the LC and HC states can be measured. The β_t values (Fig. 5b) for HC and LC states are similar and show good agreement with those found
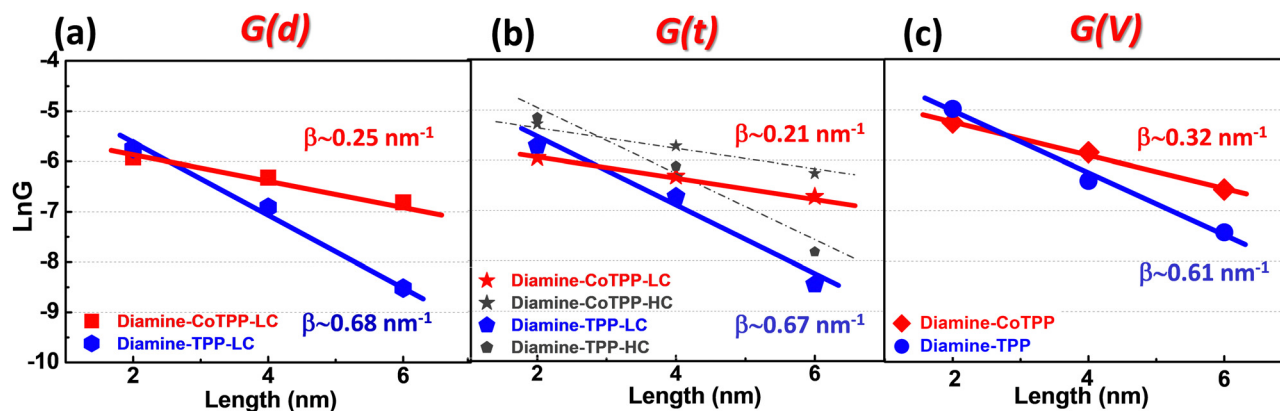

Fig. 5 Attenuation plots *vs.* thickness dependence for Au-[CoTPP]$_n$-Au and Au-[TPP]$_n$-Au SMJs (n = 1, 2, 3) using three different methods: (a) $G(d)$, (b) $G(t)$ and (c) $G(V)$ values are shown. Corresponding β factors are the slopes of the lines. Full and dashed lines are plotted from the LC and the HC values, respectively. Bias voltage: U_s = 0.025–0.2 V.

This journal is © The Royal Society of Chemistry 2024

J. Mater. Chem. C, 2024, **12**, 4326–4335 | **4331**

from the STM-bj β_d values for both Au-[CoTPP]$_n$-Au SMJs and Au-[TPP]$_n$-Au SMJs. Finally, SMJs conductance values (defined as G_{volt}) are measured from the I/V curves (Fig. 4) at low voltages (0.025 and 0.05 V) for Au-[CoTPP]$_n$-Au and Au-[TPP]$_n$-Au SMJs of different lengths. These two voltage values are chosen to calculate the attenuation factors because they are within the linear I/V ranges used for the $G(d)$ and $G(t)$ measurements. The β_v values thus calculated are 0.32 ± 0.1 nm^{-1} for Au-[CoTPP]$_n$-Au and 0.63 ± 0.1 nm^{-1} for Au-[TPP]$_n$-Au SMJs (Fig. 6c). Note that the $G(V)$ curves are usually obtained with higher noise levels due to the applied voltages (broadening of the heatmap in Fig. 4) and it is difficult to distinguish the different LC and HC states. The β_v values are thus extracted using the average values of the $G(V)$ heatmaps and show slight difference compared to β_d and β_t. A very important result is that β values (at low voltage) can thus be obtained from the different $G(d)$, $G(t)$ and $G(V)$ methods, and show good agreement, with only minor differences (± 0.1 nm^{-1}). To the best of our knowledge, β_v values have never been reported and compared to β_d and β_t previously at the single-molecule level. This also demonstrate that the I/V characteristics reported here are highly reliable.

These β values, for both the -[CoTPP]$_n$- and -[TPP]$_n$- SMJs, are rather small compared to those for conjugated SMJs in the non-resonant tunneling regime ($\beta_d \geq 2$ nm^{-1})[93] but are close to those for porphyrin-based molecular nanowires already published.[30,69,96] They show that the conductance of Au-[CoTPP]$_n$-Au is much less sensitive to the junction length (from 2 to 5.5 ± 1 nm) than that of Au-[TPP]$_n$-Au SMJs. The smaller β value for Au-[CoTPP]$_n$-Au SMJs is generally interpreted as meaning that the HOMO of CoTPP is closer to the Fermi level of the bottom gold electrodes than is that of the free base, and that this difference leads to more efficient longer-range charge transfer This suggests that the Au-[TPP]$_n$-Au SMJ is most probably dominated by non-resonant tunneling transport whereas the Au-[CoTPP]$_n$-Au SMJ has combined transport mechanisms, with both near resonant tunneling and intrachain hopping[21,22,31,32,97] (although identifying the dominant mechanism using transport measurements at various temperature is beyond the scope of this study). The cobalt ion has a

strong signature on the SMJ transport properties; this has been previously demonstrated by both the authors and other groups for similar metal-porphyrin wire systems.[69,96]

Voltage effect on attenuation factors

SMJs conductance is known to show pronounced dependence on the junction length, which is reflected by the attenuation plots. Surprisingly, less is known about how the applied bias voltage affects the attenuation factor at the single-molecule level, and only few experimental results have been reported.[44]

The Au-[CoTPP]$_n$-Au or Au-[TPP]$_n$-Au SMJ I/V curves (each averaged from five individual curves) at three different oligomer lengths are superimposed in inset images of Fig. 6a and b. To understand the bias-driven conductance variations, the β_v values (Fig. S14, ESI†) have been calculated at different bias voltages, by the method described in Fig. 5c. The β_v *versus* voltage variations are depicted in Fig. 6a and b for both the Au-[CoTPP]$_n$-Au and the Au-[TPP]$_n$-Au SMJs.

For Au-[CoTPP]$_n$-Au SMJs (Fig. 6a) the β_v value is initially very small (0.3 nm^{-1} at ± 0.05 V). The β_v values appear to plateau at voltages below ± 0.1 V, the voltage range used for STM-bj measurements. SMJ conductance shows a very weak response to voltage changes. This is also the voltage range where the I/V curves in Fig. 5 appear linear. When the bias voltage increases (negative or positive), the β_v values fall to about 0.2 nm^{-1} at ± 0.3 V bias (I/V saturation). If this trend continues, as shown by the blue fitting (Fig. 6a) β_v is predicted to reach as little as 0.1 nm^{-1} at ± 0.6 V. For Au-[CoTPP]$_n$-Au SMJ, β_v shows a voltage-dependent decrease with applied bias voltage. This decrease, at both negative and positive voltages, can most probably be attributed to a narrowing of the HOMO- (or LUMO)-Fermi level gap as the bias voltage increases. These very small β_v values and the continuous decrease suggest that resonant tunneling is the dominant transport mechanism at the bias voltages applied with a plausible contribution from redox hopping.

The β_v for Au-[TPP]$_n$-Au SMJs depends also on the applied bias voltage (Fig. 6b) in the voltage range investigated. The β_v values are around 0.6 nm^{-1} at ± 0.05 V and fall to 0.45 nm^{-1}
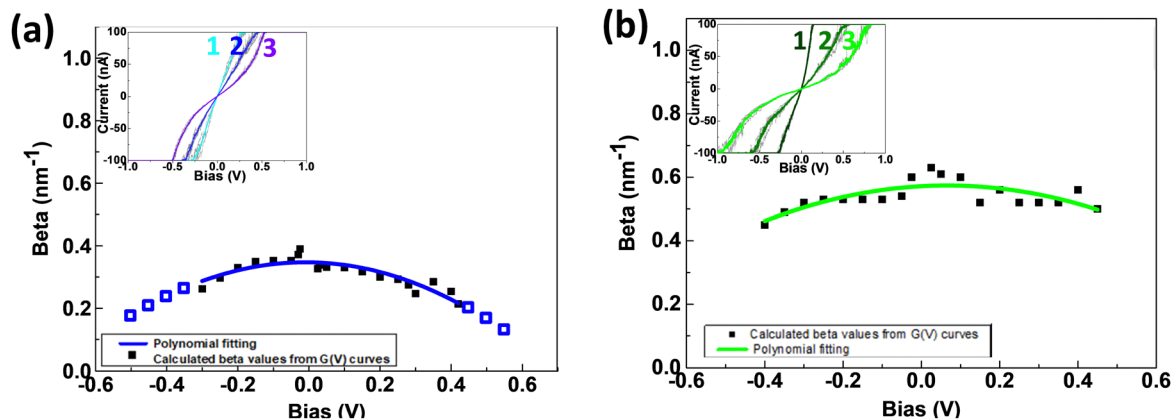

Fig. 6 Attenuation factor β_v *versus* voltage of (a) Au-[CoTPP]$_n$-Au and (b) Au-[TPP]$_n$-Au SMJs calculated from I/V curves (for three different lengths, inset images). Black square points are extrapolated values from I/V curves at different bias voltages.

4332 | *J. Mater. Chem. C*, 2024, **12**, 4326–4335

This journal is © The Royal Society of Chemistry 2024

at ± 0.5 V, which are larger values than for Au-$[CoTPP]_n$-Au SMJs. The applied voltages, up to ± 0.5 V, seem to be too low to greatly modify the β_v trends. This can be understood, as -$[TPP]_n$- has a larger HOMO–LUMO gap than -$[CoTPP]_n$-; therefore, the applied bias voltage (I/V saturation at ± 0.5 V) is not sufficient to reach resonant transport. With the voltage range used in our experiments, non-resonant tunneling remains the main transport mechanism.

Conclusions

Overall, we have fabricated $[CoTPP]_n$- and $[TPP]_n$-based SMJs at three different junction lengths (2, 4 and 6 nm $\pm$ 1 nm) using STM. The oligo-porphyrins are covalently bonded, mostly perpendicularly to the bottom Au electrode, and a top NH_2 unit acts as an anchoring group for the STM tip. The conductance of the Au-$[CoTPP]_n$-Au and Au-$[TPP]_n$-Au (n = 1, 2, 3) SMJs has been characterized by the STM-bj $G(d)$ technique and STM $G(t)$ measurements. Due to both the diazonium-generated covalent bonding to the bottom electrode and the active anchoring to the top STM tip, the Au-$[CoTPP]_1$-Au SMJs are repeatedly stabilized with a long lifetime (for STM-based SMJs at room temperature), up to 1 min, before total breakdown. Using our strategy for fabrication, it is thus easy to obtain long-lived SMJs which allow reliable I/V characterization at the single-molecule level. The obtained results indicate the essential roles of the additional NH_2 anchoring group and its interactions with the STM-tip top-electrode.

Length-dependent transport properties have been characterized by β factors using $G(d)$, $G(t)$ and $G(V)$ analyses. The β_d and β_t values are low, around 0.3 nm^{-1} and 0.7 nm^{-1} for Au-$[CoTPP]_n$-Au and Au-$[TPP]_n$-Au SMJs, respectively. The conductance shows pronounced length dependence and a clear molecular signature at low voltage (≤ 0.2 V). The dominant transport mechanism for Au-$[TPP]_n$-Au SMJs is most probably non-resonant tunneling, whereas that for Au-$[CoTPP]_n$-Au SMJs is closer to resonant tunneling with a plausible contribution from redox hopping. Moreover, voltage-dependent β_v are obtained by analyzing I/V characterizations for all SMJs. At low voltage (≤ 0.2 V), β_v hardly varies with the voltage and are in good agreement with β_d and β_t. This clearly indicates that the I/V characteristics are reliable. At higher voltage, the variation of β_v is more pronounced. In the case of Au-$[CoTPP]_n$-Au SMJs, the clearly bent profile of β_v variation with the voltage increase is caused by a narrowing of the HOMO-(or LUMO)-Fermi level gap. The β_v is reduced below 0.2 nm^{-1} above ± 0.3 V, which suggests that, driven by the bias voltage, resonant tunneling becomes the dominant transport mechanism. The β_v for Au-$[TPP]_n$-Au SMJs has higher values and shows weaker voltage dependence than for Au-$[CoTPP]_n$-Au SMJs.

Author contributions

Conflicts of interest

There are no conflicts to declare.

References

1 S. E. Thompson and S. Parthasarathy, *Mater. Today*, 2006, **9**, 20–25.
2 M. M. Waldrop, *Nature*, 2016, **530**, 144.
3 B. Hoefflinger, in *Chips 2020: a guide to the future of nano-electronics*, ed. B. Hoefflinger, Springer Berlin Heidelberg, Berlin, Heidelberg, 2012, pp. 161–174.
4 P. Ball, *Nat. Mater.*, 2022, **21**, 132.
5 H. Jagannathan, B. Anderson, C. W. Sohn, G. Tsutsui, J. Strane, R. Xie, S. Fan, K. I. Kim, S. Song and S. Sieg, in *2021 IEEE International Electron Devices Meeting (IEDM)*, IEEE, 2021, pp. 21–26.
6 K. Terabe, T. Hasegawa, T. Nakayama and M. Aono, *Nature*, 2005, **433**, 47–50.
7 I. Valov, T. Hasegawa, T. Tsuruoka, R. Waser and M. Aono, in *Nanoscale Electrochemical Studies: How Can We Use the Atomic Switch*, ed. M. Aono, Springer International Publishing, Cham, 2020, pp. 73–93.
8 C. Schirm, M. Matt, F. Pauly, J. C. Cuevas, P. Nielaba and E. Scheer, *Nat. Nanotechnol.*, 2013, **8**, 645–648.
9 K. Krishnan, T. Tsuruoka, C. Mannequin and M. Aono, *Adv. Mater.*, 2016, **28**, 640–648.
10 P.-C. Lacaze and J.-C. Lacroix, *Non-volatile memories*, John Wiley & Sons, 2014.
11 H. Jeong, D. Kim, D. Xiang and T. Lee, *ACS Nano*, 2017, **11**, 6511–6548.
12 R. L. McCreery, H. Yan and A. J. Bergren, *Phys. Chem. Chem. Phys.*, 2013, **15**, 1065–1081.
13 A. Vilan, D. Aswal and D. Cahen, *Chem. Rev.*, 2017, **117**, 4248–4286.
14 J. C. Lacroix, *Curr. Opin. Electrochem.*, 2018, **7**, 153–160.
15 N. Xin, J. Guan, C. Zhou, X. Chen, C. Gu, Y. Li, M. A. Ratner, A. Nitzan, J. F. Stoddart and X. Guo, *Nat. Rev. Phys.*, 2019, **1**, 211–230.
16 Y. Liu, X. Qiu, S. Soni and R. C. Chiechi, *Chem. Phys. Rev.*, 2021, **2**, 21303.
17 T. A. Su, M. Neupane, M. L. Steigerwald, L. Venkataraman and C. Nuckolls, *Nat. Rev. Mater.*, 2016, **1**, 16002.
18 Y. Tanaka, Y. Kato, T. Tada, S. Fujii, M. Kiguchi and M. Akita, *J. Am. Chem. Soc.*, 2018, **140**, 10080–10084.
19 Y. Tanaka, Y. Bae, F. Ogasawara, K. Suzuki, S. Kobayashi, S. Kaneko, S. Fujii, T. Nishino and M. Akita, *Adv. Mater. Interfaces*, 2023, **10**, 1–7.
20 R. C. Chiechi, E. A. Weiss, M. D. Dickey and G. M. Whitesides, *Angew. Chem., Int. Ed.*, 2008, **47**, 142–144.

This journal is © The Royal Society of Chemistry 2024

J. Mater. Chem. C, 2024, **12**, 4326–4335 | **4333**

21 Q. Van Nguyen, P. Martin, D. Frath, M. L. Della Rocca, F. Lafolet, S. Bellinck, P. Lafarge and J. C. Lacroix, *J. Am. Chem. Soc.*, 2018, **140**, 10131–10134.

22 Q. Van Nguyen, U. Tefashe, P. Martin, M. L. Della Rocca, F. Lafolet, P. Lafarge, R. L. McCreery and J.-C. Lacroix, *Adv. Electron. Mater.*, 2020, **6**, 1901416.

23 C. A. Nijhuis, W. F. Reus and G. M. Whitesides, *J. Am. Chem. Soc.*, 2010, **132**, 18386–18401.

24 L. Yuan, L. Wang, A. R. Garrigues, L. Jiang, H. V. Annadata, M. Anguera Antonana, E. Barco and C. A. Nijhuis, *Nat. Nanotechnol.*, 2018, **13**, 322–329.

25 Y. Tanaka, Y. Kato, K. Sugimoto, R. Kawano, T. Tada, S. Fujii, M. Kiguchi and M. Akita, *Chem. Sci.*, 2021, **12**, 4338–4344.

26 Y. Han, C. Nickle, Z. Zhang, H. P. A. G. Astier, T. J. Duffin, D. Qi, Z. Wang, E. del Barco, D. Thompson and C. A. Nijhuis, *Nat. Mater.*, 2020, **19**, 843–848.

27 S. Goswami, S. P. Rath, D. Thompson, S. Hedström, M. Annamalai, R. Pramanick, B. R. Ilic, S. Sarkar, S. Hooda, C. A. Nijhuis, J. Martin, R. S. Williams, S. Goswami and T. Venkatesan, *Nat. Nanotechnol.*, 2020, **15**, 380–389.

28 I. Hnid, D. Frath, F. Lafolet, X. Sun and J.-C. Lacroix, *J. Am. Chem. Soc.*, 2020, **142**, 7732–7736.

29 I. Hnid, M. Liu, D. Frath, S. Bellynck, F. Lafolet, X. Sun and J.-C. Lacroix, *Nano Lett.*, 2021, **21**, 7555–7560.

30 Z. Li, T. H. Park, J. Rawson, M. J. Therien and E. Borguet, *Nano Lett.*, 2012, **12**, 2722–2727.

31 S. Ho Choi, B. Kim and C. D. Frisbie, *Science*, 2008, **320**, 1482–1486.

32 H. Yan, A. J. Bergren, R. McCreery, M. L. Della Rocca, P. Martin, P. Lafarge and J. C. Lacroix, *Proc. Natl. Acad. Sci. U. S. A.*, 2013, **110**, 5326–5330.

33 C. A. Martin, D. Ding, J. K. Sørensen, T. Bjørnholm, J. M. van Ruitenbeek and H. S. J. van der Zant, *J. Am. Chem. Soc.*, 2008, **130**, 13198–13199.

34 N. J. Xu and B. Q. Tao, *Science*, 2003, **301**, 1221–1223.

35 S. Fujii, M. Koike, T. Nishino, Y. Shoji, T. Suzuki, T. Fukushima and M. Kiguchi, *J. Am. Chem. Soc.*, 2019, **141**, 18544–18550.

36 Y. Li, M. Buerkle, G. Li, A. Rostamian, H. Wang, Z. Wang, D. R. Bowler, T. Miyazaki, L. Xiang, Y. Asai, G. Zhou and N. Tao, *Nat. Mater.*, 2019, **18**, 357–363.

37 L. Venkataraman, J. E. Klare, C. Nuckolls, M. S. Hybertsen and M. L. Steigerwald, *Nature*, 2006, **442**, 904–907.

38 B. Capozzi, Q. Chen, P. Darancet, M. Kotiuga, M. Buzzeo, J. B. Neaton, C. Nuckolls and L. Venkataraman, *Nano Lett.*, 2014, **14**, 1400–1404.

39 S. Gunasekaran, D. Hernangómez-Pérez, I. Davydenko, S. Marder, F. Evers and L. Venkataraman, *Nano Lett.*, 2018, **18**, 6387–6391.

40 I. Díez-Pérez, J. Hihath, Y. Lee, L. Yu, L. Adamska, M. A. Kozhushner, I. I. Oleynik and N. Tao, *Nat. Chem.*, 2009, **1**, 635–641.

41 T. Hines, I. Diez-Perez, J. Hihath, H. Liu, Z.-S. Wang, J. Zhao, G. Zhou, K. Müllen and N. Tao, *J. Am. Chem. Soc.*, 2010, **132**, 11658–11664.

42 L. Lafferentz, F. Ample, H. Yu, S. Hecht, C. Joachim and L. Grill, *Science*, 2009, **323**, 1193–1197.

43 C. Nacci, F. Ample, D. Bleger, S. Hecht, C. Joachim and L. Grill, *Nat. Commun.*, 2015, **6**, 7397.

44 E. Leary, B. Limburg, A. Alanazy, S. Sangtarash, I. Grace, K. Swada, L. J. Esdaile, M. Noori, M. T. González, G. Rubio-Bollinger, H. Sadeghi, A. Hodgson, N. Agraït, S. J. Higgins, C. J. Lambert, H. L. Anderson and R. J. Nichols, *J. Am. Chem. Soc.*, 2018, **140**, 12877–12883.

45 M. A. Reed, C. Zhou, C. J. Muller, T. P. Burgin and J. M. Tour, *Science*, 1997, **278**, 252–254.

46 C. Zhou, C. J. Muller, M. R. Deshpande, J. W. Sleight and M. A. Reed, *Appl. Phys. Lett.*, 1995, **67**, 1160–1162.

47 Y.-P. Zhang, L.-C. Chen, Z.-Q. Zhang, J.-J. Cao, C. Tang, J. Liu, L.-L. Duan, Y. Huo, X. Shao, W. Hong and H.-L. Zhang, *J. Am. Chem. Soc.*, 2018, **140**, 6531–6535.

48 M. L. Perrin, F. Prins, C. A. Martin, A. J. Shaikh, R. Eelkema, J. H. Van Esch, T. Briza, R. Kaplanek, V. Kral, J. M. Van Ruitenbeek, H. S. J. Van Der Zant and D. Dulic, *Angew. Chem.*, 2011, **123**, 11419–11422.

49 T. Böhler, J. Grebing, A. Mayer-Gindner, H. V. Löhneysen and E. Scheer, *Nanotechnology*, 2004, **15**, S465.

50 J. Ponce, C. R. Arroyo, S. Tatay, R. Frisenda, P. Gaviña, D. Aravena, E. Ruiz, H. S. J. van der Zant and E. Coronado, *J. Am. Chem. Soc.*, 2014, **136**, 8314–8322.

51 Y. Kim, H. Song, F. Strigl, H. F. Pernau, T. Lee and E. Scheer, *Phys. Rev. Lett.*, 2011, **106**, 2–5.

52 P. Gehring, J. M. Thijssen and H. S. J. van der Zant, *Nat. Rev. Phys.*, 2019, **1**, 381–396.

53 L. A. Zotti, T. Kirchner, J. C. Cuevas, F. Pauly, T. Huhn, E. Scheer and A. Erbe, *Small*, 2010, **6**, 1529–1535.

54 M. El Abbassi, S. Sangtarash, X. Liu, M. L. Perrin, O. Braun, C. Lambert, H. S. J. van der Zant, S. Yitzchaik, S. Decurtins, S. X. Liu, H. Sadeghi and M. Calame, *Nat. Nanotechnol.*, 2019, **14**, 957–961.

55 C. Jia, B. Ma, N. Xin and X. Guo, *Acc. Chem. Res.*, 2015, **48**, 2565–2575.

56 C. Jia, A. Migliore, N. Xin, S. Huang, J. Wang, Q. Yang, S. Wang, H. Chen, D. Wang, B. Feng, Z. Liu, G. Zhang, D. H. Qu, H. Tian, M. A. Ratner, H. Q. Xu, A. Nitzan and X. Guo, *Science*, 2016, **352**, 1443–1445.

57 Z. Tan, D. Zhang, H. R. Tian, Q. Wu, S. Hou, J. Pi, H. Sadeghi, Z. Tang, Y. Yang, J. Liu, Y. Z. Tan, Z. Bin Chen, J. Shi, Z. Xiao, C. Lambert, S. Y. Xie and W. Hong, *Nat. Commun.*, 2019, **10**, 4–10.

58 N. Xin, C. Hu, H. Al Sabea, M. Zhang, C. Zhou, L. Meng, C. Jia, Y. Gong, Y. Li and G. Ke, *J. Am. Chem. Soc.*, 2021, **143**, 20811–20817.

59 L. Meng, N. Xin, C. Hu, H. Al Sabea, M. Zhang, H. Jiang, Y. Ji, C. Jia, Z. Yan and Q. Zhang, *Nat. Commun.*, 2022, **13**, 1–6.

60 C. Yang, L. Zhang, C. Lu, S. Zhou, X. Li, Y. Li, Y. Yang, Y. Li, Z. Liu and J. Yang, *Nat. Nanotechnol.*, 2021, **16**, 1214–1223.

61 X. Xie, P. Li, Y. Xu, L. Zhou, Y. Yan, L. Xie, C. Jia and X. Guo, *ACS Nano*, 2022, **16**, 3476–3505.

4334 | *J. Mater. Chem. C*, 2024, **12**, 4326–4335

This journal is © The Royal Society of Chemistry 2024

62 W. Haiss, R. J. Nichols, H. van Zalinge, S. J. Higgins, D. Bethell and D. J. Schiffrin, *Phys. Chem. Chem. Phys.*, 2004, **6**, 4330–4337.

63 S. Chang, J. He, L. Lin, P. Zhang, F. Liang, M. Young, S. Huang and S. Lindsay, *Nanotechnology*, 2009, **20**, 185102.

64 A. C. Aragonès, N. Darwish, W. J. Saletra, L. Pérez-García, F. Sanz, J. Puigmartí-Luis, D. B. Amabilino and I. Díez-Pérez, *Nano Lett.*, 2014, **14**, 4751–4756.

65 D. Kockmann, B. Poelsema and H. J. W. Zandvliet, *Nano Lett.*, 2009, **9**, 1147–1151.

66 A. C. Aragonès, N. Darwish, S. Ciampi, F. Sanz, J. J. Gooding and I. Díez-Pérez, *Nat. Commun.*, 2017, **8**, 15056.

67 C. R. Peiris, Y. B. Vogel, A. P. Le Brun, A. C. Aragonès, M. L. Coote, I. Díez-Pérez, S. Ciampi and N. Darwish, *J. Am. Chem. Soc.*, 2019, **141**, 14788–14797.

68 X. Yao, X. Sun, F. Lafolet and J.-C. Lacroix, *Nano Lett.*, 2020, **20**, 6899–6907.

69 X. Yao, M. Vonesch, M. Combes, J. Weiss, X. Sun and J.-C. Lacroix, *Nano Lett.*, 2021, **21**, 6540–6548.

70 J. Pinson and F. Podvorica, *Chem. Soc. Rev.*, 2005, **34**, 429–439.

71 D. Bélanger and J. Pinson, *Chem. Soc. Rev.*, 2011, **40**, 3995.

72 V. Stockhausen, J. Ghilane, P. Martin, G. Trippe-Allard, H. Randriamahazaka and J.-C. Lacroix, *J. Am. Chem. Soc.*, 2009, **131**, 14920–14927.

73 R. Luguya, L. Jaquinod, F. R. Fronczek, M. Grac and K. M. Smith, *Tetrahedron*, 2004, **60**, 2757–2763.

74 Z. Xue, A. Hou, D. W. Kwong and W. Wong, *Bioorg. Med. Chem. Lett.*, 2007, **17**, 4266–4270.

75 S. Baranton and D. Bélanger, *Electrochim. Acta*, 2008, **53**, 6961–6967.

76 V. Stockhausen, G. Trippé-Allard, V. Q. Nguyen, J. Ghilane and J. C. Lacroix, *J. Phys. Chem. C*, 2015, **119**, 19218–19227.

77 B. Jousselme, G. Bidan, M. Billon, C. Goyer, Y. Kervella, S. Guillerez, E. A. Hamad, C. Goze-Bac, J.-Y. Y. Mevellec and S. Lefrant, *J. Electroanal. Chem.*, 2008, **621**, 277–285.

78 F. Anariba, S. H. DuVall and R. L. McCreery, *Anal. Chem.*, 2003, **75**, 3837–3844.

79 C. A. Bessel and D. R. Rolison, *J. Phys. Chem. B*, 1997, **101**, 1148–1157.

80 V. N. Nemykin, P. Galloni, B. Floris, C. D. Barrett, R. G. Hadt, R. I. Subbotin, A. G. Marrani, R. Zanoni and N. M. Loim, *Dalton Trans.*, 2008, 4233–4246.

81 C. Agnès, J.-C. Arnault, F. Omnès, B. Jousselme, M. Billon, G. Bidan and P. Mailley, *Phys. Chem. Chem. Phys.*, 2009, **11**, 11647–11654.

82 C. Bruot, J. Hihath and N. Tao, *Nat. Nanotechnol.*, 2012, **7**, 35–40.

83 I. Diez-Perez, J. Hihath, T. Hines, Z.-S. Wang, G. Zhou, K. Müllen and N. Tao, *Nat. Nanotechnol.*, 2011, **6**, 226–231.

84 M. Kamenetska, S. Y. Quek, A. C. Whalley, M. L. Steigerwald, H. J. Choi, S. G. Louie, C. Nuckolls, M. S. Hybertsen, J. B. Neaton and L. Venkataraman, *J. Am. Chem. Soc.*, 2010, **132**, 6817–6821.

85 F. Chen, X. Li, J. Hihath, Z. Huang and N. Tao, *J. Am. Chem. Soc.*, 2006, **128**, 15874–15881.

86 L. Venkataraman, J. E. Klare, I. W. Tam, C. Nuckolls, M. S. Hybertsen and M. L. Steigerwald, *Nano Lett.*, 2006, **6**, 458–462.

87 W. Hong, D. Z. Manrique, P. Moreno-García, M. Gulcur, A. Mishchenko, C. J. Lambert, M. R. Bryce and T. Wandlowski, *J. Am. Chem. Soc.*, 2012, **134**, 2292–2304.

88 Z. F. Liu, S. Wei, H. Yoon, O. Adak, I. Ponce, Y. Jiang, W. D. Jang, L. M. Campos, L. Venkataraman and J. B. Neaton, *Nano Lett.*, 2014, **14**, 5365–5370.

89 G. Sedghi, V. M. García-Suárez, L. J. Esdaile, H. L. Anderson, C. J. Lambert, S. Martín, D. Bethell, S. J. Higgins, M. Elliott, N. Bennett, J. E. Macdonald and R. J. Nichols, *Nat. Nanotechnol.*, 2011, **6**, 517.

90 M. El Abbassi, P. Zwick, A. Rates, D. Stefani, A. Prescimone, M. Mayor, H. S. J. Van Der Zant and D. Dulić, *Chem. Sci.*, 2019, **10**, 8299–8305.

91 X. Li, J. He, J. Hihath, B. Xu, S. M. Lindsay and N. Tao, *J. Am. Chem. Soc.*, 2006, **128**, 2135–2141.

92 T. A. Su, H. Li, R. S. Klausen, N. T. Kim, M. Neupane, J. L. Leighton, M. L. Steigerwald, L. Venkataraman and C. Nuckolls, *Acc. Chem. Res.*, 2017, **50**, 1088–1095.

93 J. He, F. Chen, J. Li, O. F. Sankey, Y. Terazono, C. Herrero, D. Gust, T. A. Moore, A. L. Moore and S. M. Lindsay, *J. Am. Chem. Soc.*, 2005, **127**, 1384–1385.

94 N. Tuccitto, V. Ferri, M. Cavazzini, S. Quici, G. Zhavnerko, A. Licciardello and M. A. Rampi, *Nat. Mater.*, 2009, **8**, 41–46.

95 L. Luo, S. H. Choi and C. D. Frisbie, *Chem. Mater.*, 2011, **23**, 631–645.

96 G. Sedghi, K. Sawada, L. J. Esdaile, M. Hoffmann, H. L. Anderson, D. Bethell, W. Haiss, S. J. Higgins and R. J. Nichols, *J. Am. Chem. Soc.*, 2008, **130**, 8582–8583.

97 B. de Nijs, F. Benz, S. J. Barrow, D. O. Sigle, R. Chikkaraddy, A. Palma, C. Carnegie, M. Kamp, R. Sundararaman, P. Narang, O. A. Scherman and J. J. Baumberg, *Nat. Commun.*, 2017, **8**, 994.

This journal is © The Royal Society of Chemistry 2024

J. Mater. Chem. C, 2024, **12**, 4326–4335 | **4335**